Journal of Alloys and Compounds 506 (2010) 483–487

Contents lists available at ScienceDirect

Journal of Alloys and Compounds

journal homepage: www.elsevier.com/locate/jallcom

Epitaxial growth of $La_{0.7}Sr_{0.3}CoO_3$ thin films on $SrTiO_3$ substrates by metal–organic deposition

K. Daoudi [a,*], T. Tsuchiya [b], T. Nakajima [b], A. Fouzri [c], M. Oueslati [a]

[a] Unité de Spectroscopie Raman, Faculté des Sciences de Tunis, 2092 ElManar Tunis, Tunisia
[b] National Institute of Advanced Industrial Science and Technology (AIST), Ibaraki 305-8565, Japan
[c] Laboratoire de Physico-Chimie des Matériaux, Département de Physique, Faculté des Sciences de Monastir, 5019 Monastir, Tunisia

ARTICLE INFO

Article history:
Received 9 January 2010
Received in revised form 2 July 2010
Accepted 7 July 2010
Available online 15 July 2010

Keywords:
Cobaltite
Thin films
Epitaxial growth
MOD
TEM

ABSTRACT

$La_{0.7}Sr_{0.3}CoO_3$ thin films have been epitaxially grown on $SrTiO_3$ (0 0 1) single-crystal substrates by metal–organic deposition process. Crystallinity and morphology of the obtained films were examined in detail using X-ray diffraction and transmission electron microscopy. The evolution of the out-of-plane lattice parameter with film thickness is investigated. The critical thickness for strain relaxation is found in the 60–80 nm range. The electrical properties of the obtained films in various conditions have been investigated. By increasing the annealing temperature to 1000 °C and the film thickness to 120 nm, the electrical resistivity was decreased by several orders of magnitude. We measured a resistivity of approximately 5×10^{-4} Ω cm in a wide interval of temperature 77–320 K, making this material a promising candidate for a variety of applications.

1. Introduction

Hole-doped lanthanum cobaltite of general formula $La_{1-x}Sr_xCoO_3$ (LSCO) have created renewed research interest in the mixed valence transition metal-oxides with perovskite and related structures. Owing to their interesting magnetic and electrical properties, cobaltites in thin film forms were increasingly requested in a wide range of applications, extending from component in solid oxides fuels cells, oxygen separation membranes and electrochemical reactors, to thermoelectric devices [1–6].

Physical properties of LSCO material in bulk form are basically sensitive to the chemical composition [1,3]. However, when this material is prepared in thin film form the physical properties are sensitive to structure, oxygen content, and disorder. In particular, the interface between the films and the substrate can play an important role, giving rise to phase separated regions with different magnetic structures and affecting the transport properties especially in very thin films. Consequently, the growth method, the deposition parameters, and also the substrate-induced strain will influence the electrical and magnetic properties. The strain in epitaxial thin films can be easily manipulated by varying the film thickness or the substrate material [7]. Therefore, understanding the strain is of particular interest since it can be used to advantage in tuning film properties.

Such cobaltite thin films were usually epitaxially grown on single-crystal substrates by physical processes such as pulsed laser deposition (PLD) [7] or sputtering techniques [8], requiring high vacuum and post-annealing. Therefore, to reduce the production cost, preparation of the epitaxial LSCO thin films using a simple process is more and more required. The chemical processes such as sol–gel [9–12] or metal–organic deposition [13] does not require a vacuum system and a complex apparatus which is particularly important for several applications. During the past two decades, the epitaxial growth of various perovskite like structure oxides thin films using a metal–organic deposition (MOD) has been recognized [14–16]. The MOD is one of the promising fabrication methods of oxide films, which has great advantages of low fabrication cost, easy stoichiometry control, high deposition rate, and is easily applicable to substrates of any shape and size. High quality of epitaxy and promising physical properties of superconducting YBCO [17], manganite [18–25], tin oxide [26], tin-doped indium oxide [27] and $Pb(Zr,Ti)O_3$ [28] thin films have been already reported. For making the MOD process more universal technique for the epitaxial growth of metal-oxide thin films, we investigated in this paper the epitaxial growth of $La_{0.7}Sr0_{0.3}CoO_3$ (LSCO) thin films on $SrTiO_3$ (STO) single-crystal substrates. Therefore, using the simple and low cost MOD process to prepare epitaxial cobaltite thin films exhibiting similar physical properties with those prepared by PLD or sputtering, would be appreciated by the industrial community.

* Corresponding author. Tel.: +216 73500274; fax: +216 73500278.
E-mail address: Kais.Daoudi@fsm.rnu.tn (K. Daoudi).

0925-8388/$ – see front matter © 2010 Elsevier B.V. All rights reserved.
doi:10.1016/j.jallcom.2010.07.035

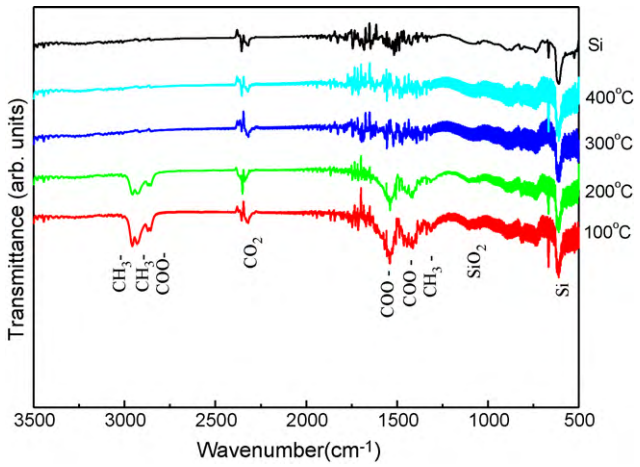

Fig. 1. IR spectra of the starting material on Si substrate heated at 100, 200, 300, and 400 °C.

2. Experimental

The LSCO thin films were prepared by a conventional MOD process. The starting solution was prepared by mixing the constituent metal-naphthenate solution (Nihon Kagaku Sangyo) and diluting with toluene to obtain the required concentration and viscosity. The molar ratios of La, Sr and Co in the coating solution were 0.7, 0.3 and 1.0, respectively. This solution was spin-coated onto (0 0 1) single-crystal STO substrates at 4000 rpm for 10 s. To eliminate the toluene, the metal–organic (MO) film was then dried in air at 100 °C for 10 min. Before the final annealing, a preheating step at 500 °C for 30 min is necessary to decompose the organic part. The preheating step is also required to prevent the formation of fissures on the film surface during the final thermal annealing at high temperature. To obtain a satisfactory film thickness, the above procedure (coating, drying, and preheating) was repeated several times (up to 5–6 times) giving rise to a corresponding number of superimposed layers in the LSCO product film. The final annealing was carried out in a conventional furnace at 600–1000 °C for 60 min in air.

The residual organic components of the metal–organic and/or amorphous LMO films were analyzed by Fourier transform infrared spectroscopy (FT-IR) monitored by a Perkin-Elmer spectrum. The crystallinity and epitaxy of the obtained films were examined by X-ray diffraction analysis (XRD; MAC Science, MXP3A) θ–2θ scans, and pole-figure analysis using the Schulz reflection method. The cross-section transmission electron microscopy (XTEM) observations were performed using a high resolution electron Hitachi H-9000 microscope operated at 300 kV. The XTEM specimens were prepared following the conventional method, i.e., mechanical cutting, face-to-face gluing, mechanical grinding, polishing and dimpling, followed by Ar-ion milling at 4 kV. The resistivity–temperature (ρ–T) curves were measured by the usual DC four-probe method and by cooling the samples from 320 K to liquid nitrogen temperature (77 K).

3. Results and discussion

3.1. Crystallinity and morphology of the films

To confirm the metal–organic decomposition during the preheating process we examined the IR spectra of the LSCO film deposited on Si substrate and heated at various temperatures (100, 200, 300, and 400 °C) for 10 min. As can be seen in Fig. 1, after a short thermal annealing for 10 min at 300 °C the absorption peaks due to the presence of CH_3– and COO– disappeared completely, indicating a complete decomposition of the metal–organic compounds. On the other hand, no crystallization of the films heated in the temperature range 300–500 °C was observed in the X-ray diffraction measurements. Therefore, the metal (La, Sr or Co) naphthenate were decomposed by heating at 500 °C for 10 min, and converted to an amorphous oxide.

To follow the crystallinity evolution during the thermal annealing we show in Fig. 2 the θ–2θ XRD scans of the LSCO films obtained at various thermal annealing temperatures (600, 800, and 1000 °C). The LSCO films were obtained by repeating the spin-coating, drying and preheating cycle two times and finally crystallized with a thermal annealing at various temperatures for 60 min in air. The in-plane lattice mismatch between the LSCO film and the STO substrate is calculated by $\delta = (c_b - c_s)/c_s$, where $c_b = 3.82$ å is the bulk lattice parameter of the film material and $c_s = 3.905$ å is the bulk lattice parameter for the STO substrate [7,28]. The lattice mismatch

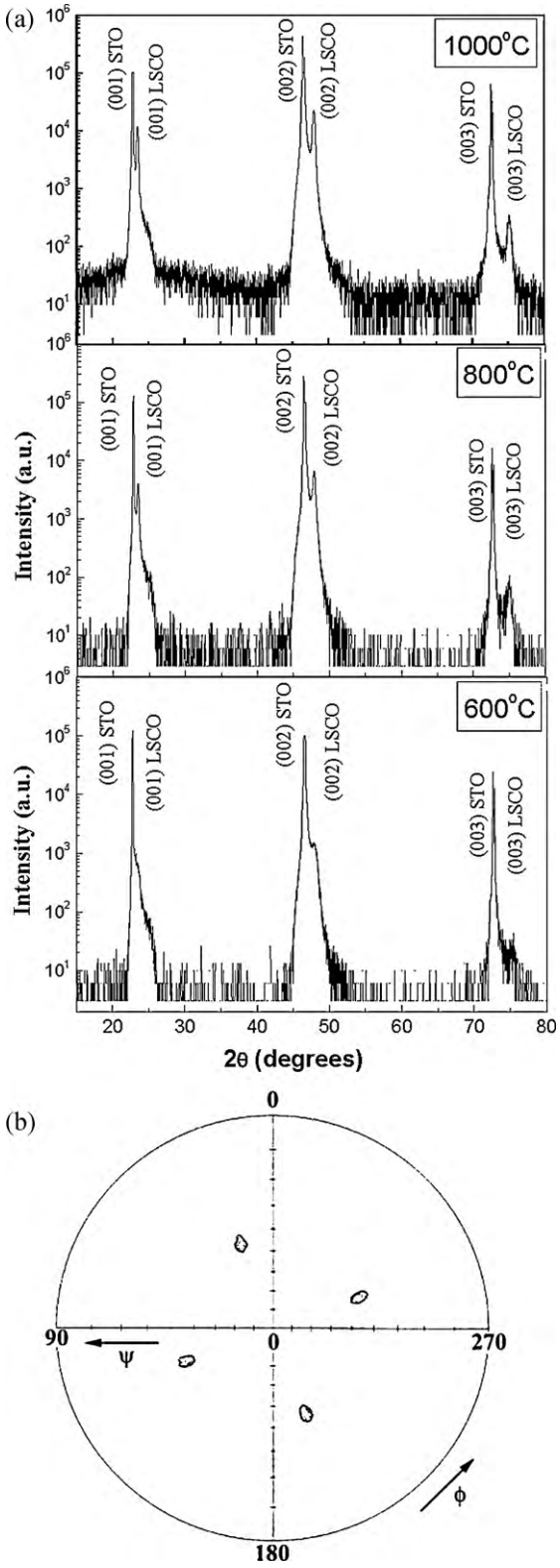

Fig. 2. (a) XRD θ–2θ scan profiles of the 40 nm thick LSCO films grown on STO (0 0 1) substrates by MOD at different temperatures (600, 800, and 1000 °C). (b) XRD pole-figure of the LSCO film annealed at 800 °C in air for 60 min.

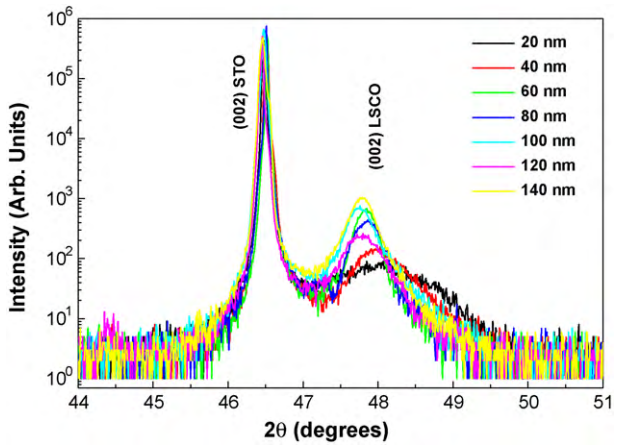

Fig. 3. θ–2θ scans close to the (0 0 2) reflection of LSCO and that of STO for samples having different thicknesses (20, 40, 60, 80, 100, 120, and 140 nm). (For interpretation of the references to colour in this figure, the reader is referred to the web version of the article.)

of the LSCO/STO system is around −2.17%. The LSCO films display clear (0 0 l) reflections of the pseudocubic structure with no indications of impurities or misorientations. Since the XRD θ–2θ cannot provide information on the in-plane alignment, we performed XRD pole-figure analysis using the Schulz reflection method to investigate the in-plan alignment of the LSCO films. Fig. 2(b) shows the XRD pole-figure of the LSCO 2 2 0 reflection for the film grown on STO substrate with a thermal annealing at 800 °C. As shown in Fig. 2(b), four sharp spots of the LSCO (2 2 0) reflections were observed every 90°. Therefore, the LSCO film is epitaxially grown on the STO substrate.

By increasing the annealing temperature from 600 to 1000 °C, we note an increase of the (0 0 l) peaks intensities (Fig. 2(a)), indicating a probable improvement of the films crystallinity. In fact, a clear estimation of the crystallinity of the film with intensity of the diffraction lines remains difficult and should be referred to the substrate peak for a clear estimation (misalignment, offset value, illuminated region.). Any way, we can just conclude from the evolution of the XRD θ–2θ scans with annealing temperature (Fig. 2(a)), that the film annealed at 600 °C exhibits a low crystallinity which is probably due to an important amount of the amorphous phase. By increasing the annealing temperature, the amorphous film is being converted to an epitaxial phase of LSCO. The percentage of the amorphous phase could play an important role in the transport properties. The out-of-plane parameters can be determined from the symmetric XRD θ–2θ scans. By increasing the annealing temperature from 600 to 1000 °C, the calculated lattice parameter of the LSCO film (c_f) increases slowly from 3.787 to 3.792 å, but do not reach the 3.82 å of the bulk material. This is probably due to the large lattice strain in the 40 nm thick film. Therefore, the discussion of the evolution of the out-of-plane lattice parameter as a function of the film thickness is much interesting. In fact, it is well known that in the films, there is a relaxation of strains from the interface towards the surface. Therefore, we show in Fig. 3 the θ–2θ XRD scans close to the (0 0 2) reflection of LSCO and that of STO for samples having various thicknesses. A noticeable peak broadening is observed for the 20 and 40 nm thick films. This broadening has been reported previously in LSCO thin films and attributed to the finite-size effect [8,30]. By increasing the film thickness from 40 to 60 nm, the peak broadening disappears, indicating an improvement of the crystalline quality of film. As well, a significant shift of the LSCO peak position toward lower angles as film thickness increases is observed. This shift corresponds to a decrease of the out-of-plan cell parameter and consequently to a progressive relaxation of the in-plane compressive strain as film thickness increases (Fig. 4). The out-of-plane parameters have been determined from the θ–2θ XRD scans are plotted as function of the film thickness (Fig. 4(a)). The c parameter is obviously increased by increasing the film thickness from 20 to 60 nm. Over a film thickness of 80 nm, the c parameter remains roughly unchanged at a value of 3.805 å. The out-of-plane epitaxial strain is calculated as $\varepsilon_{zz} = (c - c_b)/c_b$, where c is the out-of-plane lattice parameter of the film and c_b is the bulk pseudocubic lattice parameter of LSCO. The epitaxial strain ε_{zz} is plotted in Fig. 4(b) as function of the film thickness. From the evolution of the out-of-plane lattice parameter c and the epitaxial strain ε_{zz}, we can estimate the critical thickness (d_c) of strain relaxation to be in the range from 60 to 80 nm. Fuchs et al. [29,30] reported similar results concerning the LSCO prepared by PLD process and the critical thickness is found around 50 nm.

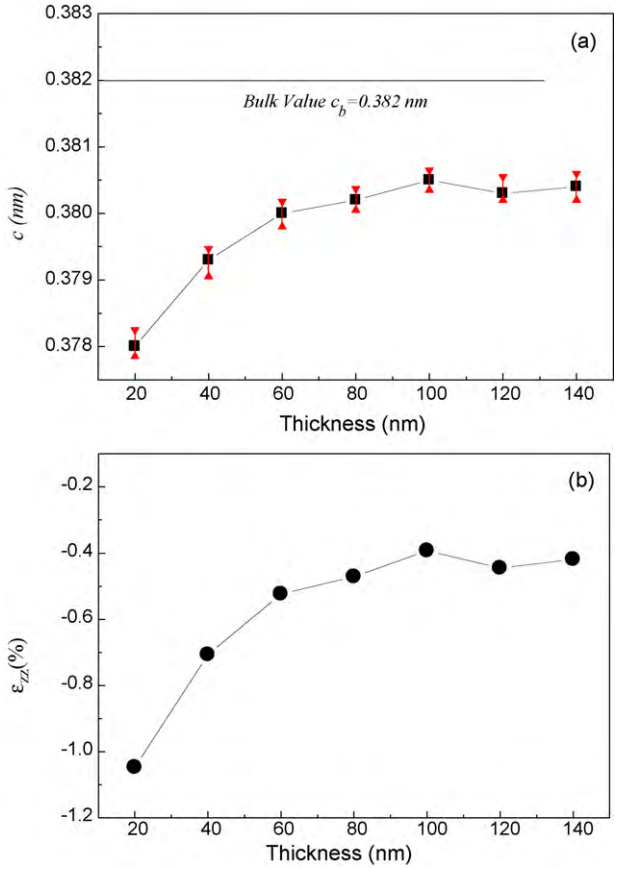

Fig. 4. (a) Out-of-plane lattice parameter c and (b) epitaxial strain ε_{zz} of LSCO as a function of the film thickness.

To have an idea about the film thickness and to better understand the epitaxial growth we carried out TEM observations on cross-section of an LSCO films prepared by MOD with a thermal annealing at 1000 °C. The cross-section TEM image of the LSCO film grown by repeating the coating, drying, and preheating cycle two times and finally annealed at 1000 °C on STO substrate is shown in Fig. 5(a). In our previous studies of the $La_{0.7}Ca_{0.3}MnO_3$ (LCMO) or $La_{0.7}Ba_{0.3}MnO_3$ (LBMO) films obtained by MOD process, one-deposited layer is found to be 20 nm thick [20,24]. This result is also confirmed here and the two-layer LSCO film thickness is around 40 nm. According to the low magnification image (Fig. 5(a)) we noted a flat surface as well as good in-depth homogeneity without any significant microstructural defects. On the other hand the LSCO/STO interface is not so sharp and in some parts is not well distinguished (Fig. 5(a)). Similar results have been observed on the LCMO and LBMO films grown on STO substrates by MOD [20,24].

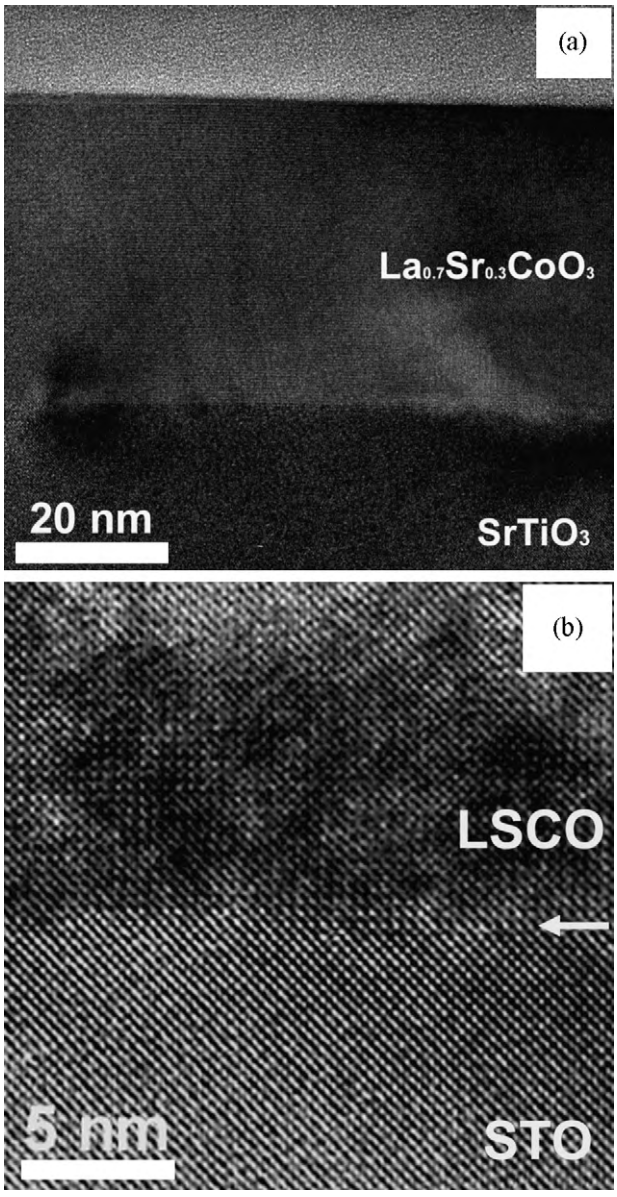

Fig. 5. Low magnification XTEM image (a) and high resolution TEM image (b) of the two-layer LSCO film grown on STO substrate by MOD at 1000 °C for 60 min in air.

In fact, the LSCO film is deposited on STO substrate by MOD using a thermal annealing at 1000 °C, which is a relatively high temperature. Therefore, during the thermal annealing at the metal–organic film/STO interface, a chemical reaction would have occurred, inducing a change in the LSCO film composition and then, the interface will not be well defined. This result is well confirmed in the HRTEM image shown in Fig. 5(b), in which the interface indicated by an arrow is not well distinguished. The HRTEM observation confirms the epitaxial growth of the LSCO film on the STO substrate. The lattice mismatch can be accommodated either by straining the lattices or by the formation of misfit dislocations at the interface depending on the elastic properties of the materials and the film thickness [31,32]. The HRTEM observations along the LCMO/STO interface indicate a good epitaxy throughout the entire film without dislocations (Fig. 5(b)). However, in both TEM images (Fig. 5(a) and (b)) we can find some defects in the form of local tweed patterns or inhomogeneous fringes distribution. In comparison with LSCO films produced by PLD process, our films prepared by the MOD process presents some deficiencies in the epitaxial quality. This is probably due to the growth process. In fact, the epitaxial growth by PLD

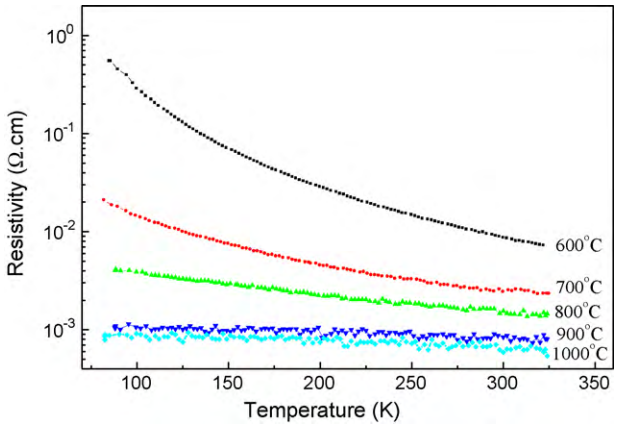

Fig. 6. $\rho(T)$ curves of the 5-layer LSCO films grown on STO substrates by MOD process at different annealing temperatures (600–1000 °C).

is generally performed layer by layer leading to high quality film. However, the epitaxial film prepared by MOD process is obtained by converting the whole deposited amorphous metal–organic film to epitaxial one using a thermal annealing treatment. Therefore, the final MOD film may contain an important amorphous phase which may be observed in high resolution TEM images. Further investigation of the microstructural properties of these LSCO films prepared by MOD process is necessary.

3.2. Electrical properties

For a variety of applications of the cobaltite films, it is a necessary condition that the films are conductive. Therefore, we measured the temperature dependence of resistivity (ρ) of the obtained films over a wide range of temperature (77–300 K). Fig. 6 shows $\rho(T)$ curves for the LSCO films grown on STO substrates by MOD with various annealing temperatures (600–1000 °C). The electrical resistivity for LSCO films decreases systematically by increasing the annealing temperature. A semiconducting-like ($d\rho/dT < 0$) behavior is observed over the whole temperature range for different annealing temperatures. Rata et al. [7] studied the transport properties of LSCO films deposited by PLD process on various substrates. The 60 nm thick LSCO film deposited on $LaAlO_3$ substrate displays metallic conductivity at all temperatures, which is comparable with bulk behavior, e.g., $\rho(5\,K) \simeq 1.2 \times 10^{-4}\,\Omega\,cm$. The same film deposited on $Pb(Mg_{1/3}Nb_{2/3})_{0.72}Ti_{0.28}O_3$ (PMN-PT) substrate exhibits a semiconducting behavior with $\rho(300\,K) \simeq 40\,\Omega\,cm$. The LSCO/STO film with larger tensile strain had a gigaohm resistance at 300 K. Therefore, the strain induced by the substrate would be the major responsible for these important conductivity variations among the films. In our case, for the 40 nm thick films prepared by MOD process at various annealing temperatures on STO substrates, the room temperature resistivity decreases from 8.5×10^{-3} to $5.9 \times 10^{-4}\,\Omega\,cm$ by increasing the annealing temperature from 600 to 1000 °C. Therefore, increasing the annealing temperature from 600 to 1000 °C decreases the film resistivity at room temperature by one order of magnitude. At low temperature, for example at 85 K, the resistivity values decrease from 0.28 to $0.91 \times 10^{-3}\,\Omega\,cm$ by increasing the annealing temperature from 600 to 1000 °C. In effect, this enhancement of the transport properties may be due to an improvement of the film crystallinity by increasing the annealing temperature. According to the XRD analysis (Section 3.1), the LSCO film annealed at 1000 °C is the best crystallized one and contain the lowest amorphous amount when compared to the films annealed at lower temperatures. However its transport behavior is still semiconducting and not metallic as compared to the bulk or those films prepared by PLD process [7,32–34]. This is probably due

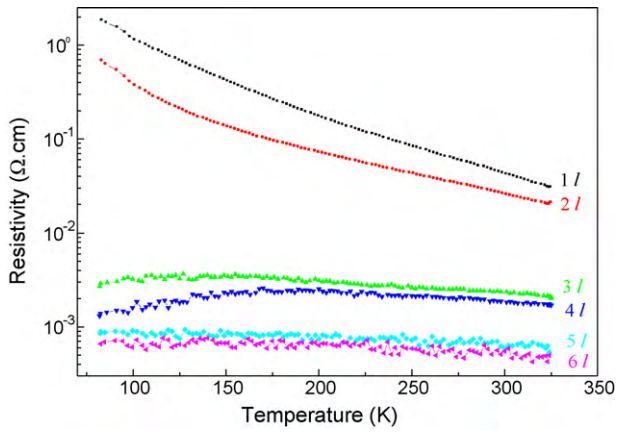

Fig. 7. $\rho(T)$ curves of the LSCO films with various thicknesses grown on STO substrates by MOD with a thermal annealing at 1000 °C for 60 min in air.

to the low oxygen content and presence of amorphous phase in our films produced by MOD.

The effects of the cobaltite film thickness on the microstructural, electrical and magnetic properties are well investigated by Fuchs et al. [29,30]. They demonstrated a rapid increase in the Curie temperature (T_c) for the film thicknesses less than 100 nm, and then stabilized around the bulk $T_c \approx 240$ K for higher thicknesses [30]. The very thin film (2.6 nm) exhibits a very high resistivity and almost bulk behavior for 10 nm films (metallic with a small change near the magnetic transition). In our case, the 20 and 40 nm thick LSCO films exhibited a semiconducting-like behavior in the whole temperature interval (Fig. 7). However, more than three deposited layers films (≥60 nm), the LSCO exhibited a usual cobaltite $\rho(T)$ curves characterized by a broad transition from a metallic state to a semiconducting state. This result might be explained by the strain relaxation by increasing the film thickness higher than a critical film thickness (Fig. 3). The 100 nm thick film annealed at 1000 °C exhibit similar $\rho(T)$ behavior to the 10 nm thick film prepared by PLD process. Therefore, when using the MOD process the presence of amorphous phases, oxygen deficiency, and defects may play important roles controlling the electrical transport in the films. For several applications of LSCO films as electrodes it is important to note, that our films exhibited good values of resistivity. The one-layer deposited LSCO film (20 nm) exhibited a resistivity of 1.830 Ω cm at 85 K and decreases to reach 30×10^{-3} Ω cm at room temperature. An increase in the film thickness from 20 to 100–120 nm (5–6 layers) is followed by a decrease in the film resistivity from 1830 to 6×10^{-4} Ω cm at 85 K, and from 30.4×10^{-3} to 5×10^{-4} Ω cm at room temperature. Finally the 120 nm LSCO film annealed at 1000 °C shows a rather constant resistivity of $(5–6) \times 10^{-4}$ Ω cm in the whole temperature interval between 77 and 320 K.

The 3 layer (60 nm) and 4 layer (80 nm) LSCO films show broad transitions. However, for the thicker ones (5 layers and 6 layers), the ferromagnetic transition is not easily distinguished. At this stage of investigation we cannot provide a precise explanation of this result. Therefore, further investigations of the magnetic properties are necessary to determine the precise values of ferromagnetic transition (T_c) for various LSCO films prepared by MOD process.

4. Conclusion

We have successfully prepared epitaxial LSCO thin films on STO single-crystal substrate using a metal–organic deposition process. The organic compounds were easily removed by a short thermal annealing at less than 300 °C. By increasing the annealing temperature from 600 to 1000 °C, the film crystallinity is enhanced. The critical thickness for film strain relaxation is found to be in the 60–80 nm range. The LSCO film shows a good epitaxial quality without dislocations or defects. The annealing temperature plays a key role on the electrical properties of the LSCO, and annealing at higher than 900 °C is necessary to obtain good values of resistivity. The electrical resistivity values are rather constant in a wide temperature interval between 77 and 300 K for the totally relaxed films with a thickness over 60 nm.

References

[1] P.M. Raccah, J.B. Goodebough, J. Appl. Phys. 39 (1968) 1209.
[2] C.N.R. Rao, D. Om Parkash, P. Bahadur, S. Ganguly, Nagabhushana, J. Solid State Chem. 22 (1977) 353.
[3] H. Taguchi, M. Shimada, M. Koizumi, J. Solid State Chem. 33 (1980) 169.
[4] B.C.H. Steele, Solid State Ionics 86–88 (1996) 1223.
[5] K.R. Kendall, C. Navas, J.K. Thomas, H.C. zur Loye, Chem. Mater. 8 (1996) 642.
[6] H.D. Bhatt, R. Vedula, S.B. Desu, G.C. Fralick, Thin Solid Films 350 (1999) 249.
[7] A.D. Rata, A. Herklotz, K. Nenkov, L. Schultz, K. Dorr, Phys. Rev. Lett. 100 (2008) 076401.
[8] M.A. Torija, M. Sharma, M.R. Fitzsimmons, M. Varela, C. Leighton, J. Appl. Phys. 104 (2008) 023901.
[9] M. Popa, J.M.C. Moreno, Thin Solid Films 517 (2009) 1530.
[10] L. Armelao, D. Barreca, G. Bottaro, A. Gasparotto, C. Maragno, E. Tondello, Chem. Mater. 17 (2005) 427.
[11] C. Tealdi, M. Saiful Islam, C.A.J. Fisher, L. Malavasi, G. Flor, Prog. Solid State Chem. 35 (2007) 491.
[12] D. Berger, N.V. Landschoot, C. Ionica, F. Papa, V. Fruth, J. Optoelectron. Adv. Mater. 5 (2003) 337.
[13] S. Wang, Z. Zhang, L. He, M. Chen, W. Yu, G. Fu, Appl. Phys. Lett. 94 (2009) 162108.
[14] A. Gupta, R. Jagannathan, E.I. Cooper, E.A. Giess, J.I. Landman, B.W. Hussey, Appl. Phys. Lett. 52 (1988) 2077.
[15] T. Manabe, W. Kondo, S. Mizuta, T. Kumagai, Appl. Phys. Lett. 60 (1992) 3301.
[16] T. Kumagai, T. Manabe, W. Kondo, S. Mizuta, K. Arai, Appl. Phys. Lett. 61 (1992) 988.
[17] T. Yamaguchi, M. Manabe, K. Sohma, W. Tsukada, T. Kondo, S. Kamiya, T. Mizuta, Kumagai, IEEE Trans. Appl. Supercond. 15 (2005) 2927.
[18] T. Manabe, T. Fujimoto, I. Yamaguchi, W. Kondo, I. Kojima, S. Mizuta, T. Kumagai, Thin Solid Films 323 (1998) 99.
[19] K. Daoudi, T. Tsuchiya, S. Mizuta, I. Yamaguchi, T. Manabe, T. Kumagai, Jpn. J. Appl. Phys. 43 (2004) L1054.
[20] K. Daoudi, T. Tsuchiya, I. Yamaguchi, T. Manabe, S. Mizuta, T. Kumagai, J. Appl. Phys. 97 (2005) 013507.
[21] K. Daoudi, T. Tsuchiya, I. Yamaguchi, T. Manabe, S. Mizuta, T. Kumagai, Appl. Surf. Sci. 247 (2005) 89.
[22] K. Daoudi, T. Tsuchiya, S. Mizuta, I. Yamaguchi, T. Manabe, T. Kumagai, Jpn. J. Appl. Phys. 44 (2005) 5129.
[23] K. Daoudi, T. Tsuchiya, I. Yamaguchi, T. Manabe, S. Mizuta, T. Kumagai, J. Electroceram. 16 (2006) 527.
[24] K. Daoudi, T. Tsuchiya, T. Nakajima, I. Yamaguchi, T. Manabe, T. Kumagai, Jpn. J. Appl. Phys. 46 (2007) 2530.
[25] T. Tsuchiya, K. Daoudi, I. Yamaguchi, T. Manabe, T. Kumagai, S. Mizuta, Appl. Surf. Sci. 247 (2005) 145.
[26] T. Tsuchiya, H. Niino, A. Yabe, I. Yamaguchi, T. Manabe, T. Kumagai, S. Mizuta, Appl. Surf. Sci. 197–198 (2002) 512.
[27] Y. Miyamoto, T. Tsuchiya, I. Yamaguchi, T. Manabe, H. Niino, A. Yabe, T. Kumagai, T. Tsuchiya, S. Mizuta, Appl. Surf. Sci. 197–198 (2002) 398.
[28] R. Caciuffo, D. Rinaldi, G. Barucca, J. Mira, J. Rivas, M.A.S. Rodriguez, P.G. Radaelli, D. Fiorani, J.B. Goodenough, Phys. Rev. B 59 (1999) 1068.
[29] D. Fuchs, O. Moran, P. Adelmann, R. Schneider, Physica B 349 (2004) 337.
[30] D. Fuchs, T. Schwarz, O. Moran, P. Schweiss, R. Schneider, Phys. Rev. B 71 (2005) 092406.
[31] J.Q. He, C.L. Jia, J. Schubert, R.H. Wang, J. Cryst. Growth 265 (2004) 241.
[32] D. Fuchs, L. Dieterle, E. Arac, R. Eder, P. Adelmann, V. Eyert, T. Kopp, R. Schneider, D. Gerthsen, H.V. Lohneysen, Phys. Rev. B 79 (2009) 024424.
[33] M.A.S. Rodriguez, J.B. Goodenough, J. Solid State Chem. 118 (1995) 323.
[34] M. Itoh, I. Natori, S. Kubota, K. Motoya, J. Phys. Soc. Jpn. 63 (1994) 1486.